Results in Physics 23 (2021) 104014

Contents lists available at ScienceDirect

Results in Physics

journal homepage: www.elsevier.com/locate/rinp

Dipole emission characteristics near a topological insulator sphere coated with a metallic nanoshell

Huai-Yi Xie [a,*], Railing Chang [b], P.T. Leung [c]

[a] Division of Physics, Institute of Nuclear Energy Research, Taoyuan County 32546, Taiwan
[b] Institute of Optoelectronic Sciences, National Taiwan Ocean University, Keelung, Taiwan
[c] Department of Physics, Portland State University, P. O. Box 751, Portland, OR 97207, USA

ARTICLE INFO

Keywords:
Topological insulator
Dipole emitters
Coupled plasmonic resonances

ABSTRACT

The modified emission characteristics of a source dipole near a metal-coated topological insulator sphere are studied with the application of axion electrodynamics in the long wavelength limit. Our focus is on the effect due to the topological magneto-electric (TME) response of the sphere and its influence on the multipolar plasmonic resonance of the metallic nanoshell. It is found that the TME response mainly affects the bonding modes of the metal shell plasmons with the lower order multipole resonances experiencing appreciable red-shifts. In addition, the TME effects can lead to either greater or smaller decay rates and lower emission frequencies, depending crucially on the frequency of the emitting dipole; but otherwise rather insensitive to the orientation of the dipole moments. These findings thus provide an alternative approach to probing the TME effects via molecular fluorescence experiments, as well as new possibility of controlling the emission properties of molecules using these novel nanoparticles.

Introduction

Topological insulators (TI) are quantum states of (2D/3D) matter with an insulating interior but conducting edge/surface states, with these boundary conducting states being protected topologically by time-reversal symmetry. Composite materials of heavy atoms such as Bi_2Te_3 can be fabricated to show TI properties due to the strong intrinsic spin-orbit coupling of the electrons in these materials [1,2]. Among the so many intriguing physical properties of these materials, their topological magneto-electric (TME) response is unique and has been studied intensively in the literature, leading to intriguing optical effects such as Faraday and Kerr rotations of incident polarized beams at THz frequencies, as recently observed in a series of ingenious experiments [3–5]. In addition, nontrivial modifications from this TME in the optical reciprocity of propagating EM waves have also been studied in recent time [6].

Aside from such TME effect on traveling electromagnetic (EM) waves, the corresponding effect on confined evanescent waves has also been studied in the literature. In particular, excitation of surface plasmons at an interface of a TI and a metal has been investigated and the effect has been found to be small depending on the square of the fine-structure constant [7]. In a recent study, we have extended such plasmonic excitation to the geometry of a spherical metallic shell with a TI core, and have observed such TME effect to be relatively more significant for the low frequency bonding modes of the metal shell [8] – leading to manifested red-shifts of these modes [7,8]. Moreover, this previous study was limited to an incident far-field source and only the dipolar response of the metal-coated TI core has been considered.

The goal of this paper is to extend our previous work [8], to the study of the TME on the near fields of the TI-metal core-shell system. We thus here consider a localized dipole emitter in the vicinity of such a metal-coated TI sphere and study how the emitting characteristics of the dipole are modified by the excitation of all orders of multipoles of the coated sphere. This problem with a dipole interacting with a TI sphere has been actively studied in the recent literature, but only limited to "bare" TI particles [9,10]. Realistic experiments can be designed via fluorescence studies of molecules adsorbed to these coated particles similar to those performed with bare metallic nanoparticles [11,12], with an eye on further manifestation of the TME effects from the TI, as well as the possibility of employing such effects for the control of the emission properties of the molecules.

Since we shall consider both the molecule-sphere distance and the size of the coated spheres are going to be small compared to the emission wavelengths of the molecule, we shall adopt a long-wavelength

* Corresponding author.
E-mail address: damoxie@iner.gov.tw (H.-Y. Xie).

https://doi.org/10.1016/j.rinp.2021.104014
Received 24 January 2021; Received in revised form 22 February 2021; Accepted 23 February 2021
Available online 2 March 2021

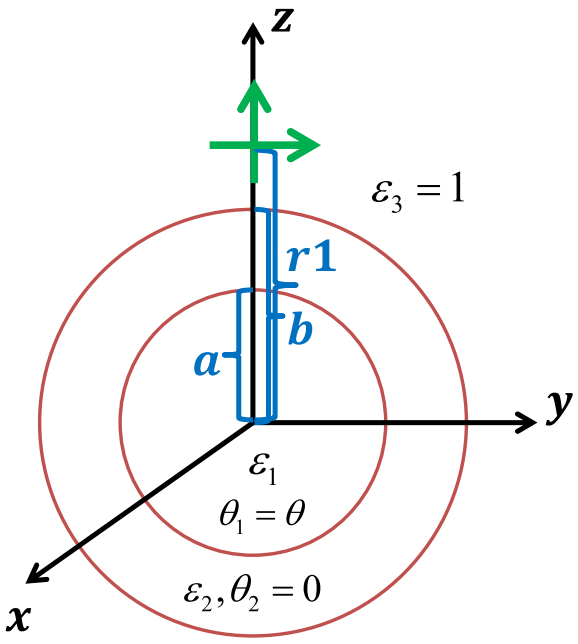

Fig. 1. Configuration of the problem: an emitting dipole with radial/tangential orientation interacting with a metallic nanoshell consisting a TI core.

formulation of the problem and all the multipolar responses of the coated sphere can be accounted for from calculating the various polarizabilities of the system. In the previous study with a far-field source, scattering experiments were referred to which require all the four (electric-electric; electric-magnetic; magnetic-electric; and magnetic-magnetic) polarizabilities to be calculated [8]. However, in our present study of near-field source in the long wavelength approximation, we will only need the electric-electric polarizability since the other three responses will only lead to higher order contributions when we study how the induced fields from the coated TI sphere will affect the source dipole.

Theory

We consider a metal shell of inner radius a and outer radius b with a TI core as shown in Fig. 1. A dipole emitter is placed on the z-axis at a radial distance r_1 outside the shell, and we consider the two mutually orthogonal orientations (radial and tangential) of the dipole. The modified Maxwell equations in axion electrodynamics in the long wavelength limit in the absence of sources were obtained previously in the literature as follows [8,13]:

$$\begin{cases} \vec{\nabla}\cdot\left(\vec{D} + 4\pi\kappa\theta\vec{B}\right) = 0 \\ \vec{\nabla}\cdot\vec{B} = 0 \\ \vec{\nabla}\times\vec{E} = 0 \\ \vec{\nabla}\times\left(\vec{H} - 4\pi\kappa\theta\vec{E}\right) = 0 \end{cases}, \tag{1}$$

where $\kappa = \frac{\alpha}{4\pi^2}$, $\alpha = \frac{e^2}{\hbar c}$ being the fine structure constant and θ is the axion field. These then lead to the following boundary conditions for the field components:

$$\begin{cases} \varepsilon_2 E_{2n} - \varepsilon_1 E_{1n} = 4\pi\kappa\theta B_n \\ B_{2n} = B_{1n} = B_n \\ E_{2t} = E_{1t} = E_t \\ B_{2t} - B_{1t} = -4\pi\kappa\theta E_t \end{cases}, \tag{2}$$

where we have assumed a linear dielectric and nonmagnetic response. By introducing scalar potentials each for the electric and magnetic field as follows:

$$\begin{cases} \vec{E} = -\vec{\nabla}\phi \\ \vec{B} = -\vec{\nabla}\phi_B \end{cases}, \tag{3}$$

the Laplace equations can then be solved subjected to the boundary conditions in (2) leading to the following results:

(i) Radial dipole

Starting with the standard general solutions for the Laplace equation and accounting for the presence of the dipole, we have:

$$\phi(\vec{r}) = \begin{cases} \sum_\ell \alpha_\ell r^\ell P_\ell(cos\Theta), r < a \\ \sum_\ell \left(\alpha'_\ell r^\ell + \beta'_\ell \frac{1}{r^{\ell+1}}\right) P_\ell(cos\Theta), a < r < b \\ -\mu\sum_\ell (\ell+1)\frac{r^\ell}{r_1^{\ell+2}} P_\ell(cos\Theta) + \sum_\ell \beta''_\ell \frac{1}{r^{\ell+1}} P_\ell(cos\Theta), b < r < r_1 \end{cases}, \tag{4}$$

and

$$\phi_B(\vec{r}) = \begin{cases} \sum_\ell s_\ell r^\ell P_\ell(cos\Theta), r < a \\ \sum_\ell \left(s'_\ell r^\ell + t'_\ell \frac{1}{r^{\ell+1}}\right) P_\ell(cos\Theta), a < r < b \\ \sum_\ell t''_\ell \frac{1}{r^{\ell+1}} P_\ell(cos\Theta), b < r < r_1 \end{cases}, \tag{5}$$

$$\begin{pmatrix} -\varepsilon_1\ell a^{\ell-1} & -A\ell a^{\ell-1} & \varepsilon_2\ell a^{\ell-1} & -\frac{\varepsilon_2(\ell+1)}{a^{\ell+2}} & 0 & 0 & 0 & 0 \\ 0 & \ell a^{\ell-1} & 0 & 0 & -\ell a^{\ell-1} & \frac{\ell+1}{a^{\ell+2}} & 0 & 0 \\ a^{\ell-1} & 0 & a^{\ell-1} & -a^{-\ell-2} & 0 & 0 & 0 & 0 \\ Aa^{\ell-1} & -a^{\ell-1} & 0 & 0 & a^{\ell-1} & a^{-\ell-2} & 0 & 0 \\ 0 & 0 & -\varepsilon_2\ell b^{\ell-1} & \frac{\varepsilon_2(\ell+1)}{b^{\ell+2}} & 0 & 0 & -\frac{\ell+1}{b^{\ell+2}} & 0 \\ 0 & 0 & 0 & 0 & \ell b^{\ell-1} & -\frac{\ell+1}{b^{\ell+2}} & 0 & \frac{\ell+1}{b^{\ell+2}} \\ 0 & 0 & -b^{\ell-1} & -b^{-\ell-2} & 0 & 0 & b^{-\ell-2} & 0 \\ 0 & 0 & 0 & 0 & -b^{\ell-1} & -b^{-\ell-2} & 0 & b^{-\ell-2} \end{pmatrix} \begin{pmatrix} \alpha_\ell \\ s_\ell \\ \alpha'_\ell \\ \beta'_\ell \\ s'_\ell \\ t'_\ell \\ \beta''_\ell \\ t''_\ell \end{pmatrix} = \begin{pmatrix} 0 \\ 0 \\ 0 \\ 0 \\ \frac{\mu\ell(\ell+1)b^{\ell-1}}{r_1^{\ell+2}} \\ 0 \\ \frac{\mu(\ell+1)b^{\ell-1}}{r_1^{\ell+2}} \\ 0 \end{pmatrix}, \tag{6}$$

where P_ℓ is the Legendre function, Θ is the polar angle and μ is the electric dipole moment of the source. Matching the appropriate boundary conditions at $r = a$ and $r = b$, we obtain the following 8x8 matrix equation for the eight unknown coefficients $\alpha_\ell, s_\ell, \alpha_\ell^{'}, \beta_\ell^{'}, s_\ell^{'}, t_\ell^{'}, \beta_\ell^{''}, t_\ell^{''}$:

where the constant A is the universval TME parameter given by [14,15]:

$$A = 4\pi\kappa\theta = \frac{\alpha\theta}{\pi} \simeq \frac{(2N+1)}{137}, \tag{7}$$

with α the fine structure constant, and N is an integer characterizing a TI with broken time-reversal symmetry. Note that Eq. (7) is the correct form for Eq. (19) of our previous paper [8], which contains by mistake an extra factor of π [16]. In order to obtain the ℓ^{th}order polarizability, we solve for the coefficient $\beta_\ell^{''}$ in Eq. (6) and obtain:

$$\beta_{\ell,\perp}^{''} = b^{2\ell+1}\ell(\ell+1)\mu r_1^{-\ell-2}\frac{a^{2\ell+1}[\ell+\varepsilon_2(\ell+1)]\left[(\varepsilon_1-\varepsilon_2)(2\ell+1)+A^2(\ell+1)\right]+b^{2\ell+1}(\varepsilon_2-1)\left[\varepsilon_2(2\ell+1)(\ell+1)+\ell(2\ell+1)\varepsilon_1+A^2\ell(\ell+1)\right]}{a^{2\ell+1}(\varepsilon_2-1)\ell(\ell+1)\left[(\varepsilon_1-\varepsilon_2)(2\ell+1)+A^2(\ell+1)\right]+b^{2\ell+1}[1+\ell(\varepsilon_2+1)]\left\{(2\ell+1)[\varepsilon_2(\ell+1)+\varepsilon_1\ell]+A^2\ell(\ell+1)\right\}}. \tag{8}$$

$$\begin{pmatrix} -\varepsilon_1\ell a^{\ell-1} & -A\ell a^{\ell-1} & \varepsilon_2\ell a^{\ell-1} & -\frac{\varepsilon_2(\ell+1)}{a^{\ell+2}} & 0 & 0 & 0 & 0 \\ 0 & \ell a^{\ell-1} & 0 & 0 & -\ell a^{\ell-1} & \frac{\ell+1}{a^{\ell+2}} & 0 & 0 \\ a^{\ell-1} & 0 & a^{\ell-1} & -a^{-\ell-2} & 0 & 0 & 0 & 0 \\ Aa^{\ell-1} & -a^{\ell-1} & 0 & 0 & a^{\ell-1} & a^{-\ell-2} & 0 & 0 \\ 0 & 0 & -\varepsilon_2\ell b^{\ell-1} & \frac{\varepsilon_2(\ell+1)}{b^{\ell+2}} & 0 & 0 & -\frac{\ell+1}{b^{\ell+2}} & 0 \\ 0 & 0 & 0 & 0 & \ell b^{\ell-1} & -\frac{\ell+1}{b^{\ell+2}} & 0 & \frac{\ell+1}{b^{\ell+2}} \\ 0 & 0 & -b^{\ell-1} & -b^{-\ell-2} & 0 & 0 & b^{-\ell-2} & 0 \\ 0 & 0 & 0 & 0 & -b^{\ell-1} & -b^{-\ell-2} & 0 & b^{-\ell-2} \end{pmatrix} \begin{pmatrix} \alpha_\ell \\ s_\ell \\ \alpha_\ell^{'} \\ \beta_\ell^{'} \\ s_\ell^{'} \\ t_\ell^{'} \\ \beta_\ell^{''} \\ t_\ell^{''} \end{pmatrix} = \begin{pmatrix} 0 \\ 0 \\ 0 \\ 0 \\ \mu\ell\frac{b^{\ell-1}}{r_1^{\ell+2}} \\ 0 \\ \mu\frac{b^{\ell-1}}{r_1^{\ell+2}} \\ 0 \end{pmatrix} \tag{11}$$

(ii) Tangential dipole

In a similar way as in (i), we obtain for a tangential source dipole the following results for the potentials:

$$\phi(\vec{r} = \begin{cases} \sum_\ell \alpha_\ell r^\ell P_\ell^1(cos\Theta)cos\varphi, r < a \\ \sum_\ell \left(\alpha_\ell^{'} r^\ell + \beta_\ell^{'}\frac{1}{r^{\ell+1}}\right)P_\ell^1(cos\Theta)cos\varphi, a < r < b \\ -\mu\sum_\ell \frac{r^\ell}{r_1^{\ell+2}}P_\ell^1(cos\Theta)cos\varphi + \sum_\ell \beta_\ell^{''}\frac{1}{r^{\ell+1}}P_\ell^1(cos\Theta)cos\varphi, b < r < r_1 \end{cases}, \tag{9}$$

and

$$\phi_B(\vec{r} = \begin{cases} \sum_\ell s_\ell r^\ell P_\ell^1(cos\Theta)cos\varphi, r < a \\ \sum_\ell \left(s_\ell^{'} r^\ell + t_\ell^{'}\frac{1}{r^{\ell+1}}\right)P_\ell^1(cos\Theta)cos\varphi, a < r < b \\ \sum_\ell t_\ell^{''}\frac{1}{r^{\ell+1}}P_\ell^1(cos\Theta)cos\varphi, b < r < r_1 \end{cases}, \tag{10}$$

where P_ℓ^1 is the associate Legendre function with $m = 1$ and φ is the azimuthal angle. Again, matching the boundary conditions in (2) leads to the following result for the eight coefficients $\alpha_\ell, s_\ell, \alpha_\ell^{'}, \beta_\ell^{'}, s_\ell^{'}, t_\ell^{'}, \beta_\ell^{''}, t_\ell^{''}$:

Solving (11), we find that the multipolar polarizability coefficient in the tangential case can simply be expressed in terms of that in the radial case in the form: $\beta_{\ell,//}^{''} = \frac{\beta_{\ell,\perp}^{''}}{\ell+1}$. Once we obtain both the coefficient $\beta_{\ell,\perp}^{''}$ and $\beta_{\ell,//}^{''}$, the normalized decay rate and the frequency shift of the emitting dipole can then be calculated from the reflected fields from the coated TI sphere as follows [17]:

$$\widehat{b} \equiv \frac{b}{b_0} = 1 + \frac{3c^3}{2\omega^3}Im(G), \tag{12}$$

$$\Delta\widehat{\omega} \equiv \frac{\Delta\omega}{b_0} = 1 - \frac{3c^3}{4\omega^3}Re(G), \tag{13}$$

where b_0 is the decay rate in free space, ω is the emission frequency, and G is the Green function corresponding to the reflected fields from the sphere acted on the dipole and is given in the long wavelength limit by $\sum_\ell \beta_{\ell,\perp}^{''}(\ell+1)\frac{1}{r_1^{\ell+2}}$ for the radial dipole and $\sum_\ell \beta_{\ell,//}^{''}\frac{\ell(\ell+1)}{2}\frac{1}{r_1^{\ell+2}}$ for the tangential dipole, respectively.

Numerical results and discussion

To illustrate via some numerical calculation of the TME-modified

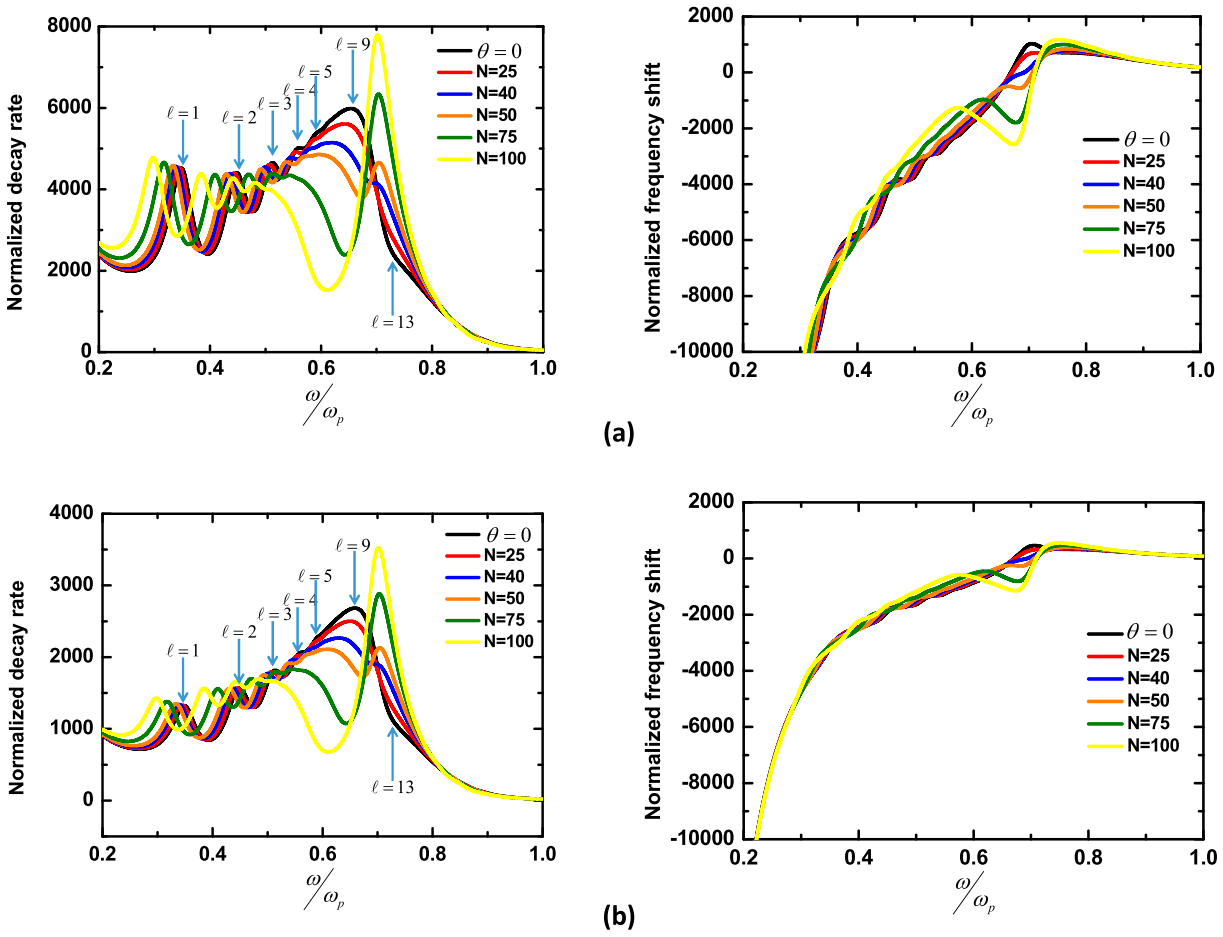

Fig. 2. Normalized decay rate and frequency shift of (a) radial and (b) tangential emitting dipole near the nanoshell as a function of the normalized emission frequency $\frac{\omega}{\omega_p}$. Note that the case with a non TI core is shown by the black line, with the inset showing the various multipole resonances (see text for details).

plasmonic effects on the emitting dipole, we start by assuming the dielectric function of the topological insulator core to be that of $TlBiSe_2$ of the following form [14]:

$$\varepsilon_1 = 1 - \frac{\omega_e^2}{\omega^2 - \omega_R^2} \tag{14}$$

with $\omega_R = 1.68 \times 10^{12}$ rad/s and $\omega_e = \sqrt{3}\omega_R$. The dielectric function of the metallic (Ag) nanoshell is described by the Drude model [18]:

$$\varepsilon_2 = 1 - \frac{\omega_p^2}{\omega^2 + i\omega\Gamma} \tag{15}$$

with the plasmon frequency $\omega_p = 1.36 \times 10^{16}$ rad/s and the damping constant $\Gamma = \Gamma_{Bulk} + \frac{\eta v_F}{b-a}$ in which $\Gamma_{Bulk} = 2.56 \times 10^{13} Hz$, $v_F = 1.39 \times 10^{15}$ nm/s and choosing $\eta = 1$.

Fig. 2 shows the results for both the normalized decay rate and emission frequency shift according to Eqs. (12) and (13) as a function of emission frequency for a dipole near a nanoshell as described above with inner radius $a = 8nm$ and outer radius $b = 10nm$. The dipole is at a fixed distance of $r_1 = 12nm$, and the case with a non-TI core ($\theta = 0$, in black) is set as a reference for the TME effects. For this case, we have analysed the various peaks in this figure and have identified one antibonding modes ($\ell = 13$, $\omega \sim 0.72\omega_p$) and six bonding modes ($\ell = 1$, $\omega \sim 0.35\omega_p$; $\ell = 2$, $\omega \sim 0.45\omega_p$; $\ell = 3$, $\omega \sim 0.51\omega_p$; $\ell = 4$, $\omega \sim 0.55\omega_p$; $\ell = 5$, $\omega \sim 0.59\omega_p$; $\ell = 9$, $\omega \sim 0.66\omega_p$) corresponding to different multipolar resonances. It can be seen that the TME effect leads to red-shifts for the low order bonding modes while those for the corresponding antibonding modes are quite insignificant. In addition, for higher order multipoles, the bonding and antibonding modes become closer and closer to each other as in the case of hollow nanoshells [18], and the red-shifts to these after a summation over many of them can hardly be distinguished from the total decay rates and induced frequency-shifts. In general, it is observed that the TME effect is not particular sensitive to the dipole orientation with very similar effects for both radial (Fig. 2(a)) and tangential (Fig. 2(b)) dipoles; except that the tangential dipole experiences overall smaller effects which can be understood from the relative opposite orientations between the source and the image, when the dipole is aligned tangentially along the spherical surface. This relative orientation between the source and the image for both the radial and tangential dipoles also leads to a negative dipole-dipole interaction energy which accounts for the red-shifted emission frequencies shown in the figure.

In order to understand better how the TME effect affects the various bonding modes of different multipole orders, we compare in Fig. 3 the cases between two multipolar resonances: $\ell = 1$ and $\ell = 11$, respectively. Only results for a radial dipole are shown here. While it is clear that monotonic increasing red-shifts are induced by the TME effect for both multipole resonances, the amplitudes contributing to the decay rate from the bonding and antibonding modes are affected quite differently: with that from the antibonding mode clearly increases with N for both $\ell = 1$ and $\ell = 11$, that from the bonding mode turns out to decrease with N with the decrease rather insignificant for the $\ell = 1$ mode. This may account for some of the features in the results shown in Fig. 2 both at the low frequency and at the high frequency regimes.

Finally we look at the distance-dependence of the decay rate of the emitting dipole as shown in Fig. 4. It is clear that while both radial and

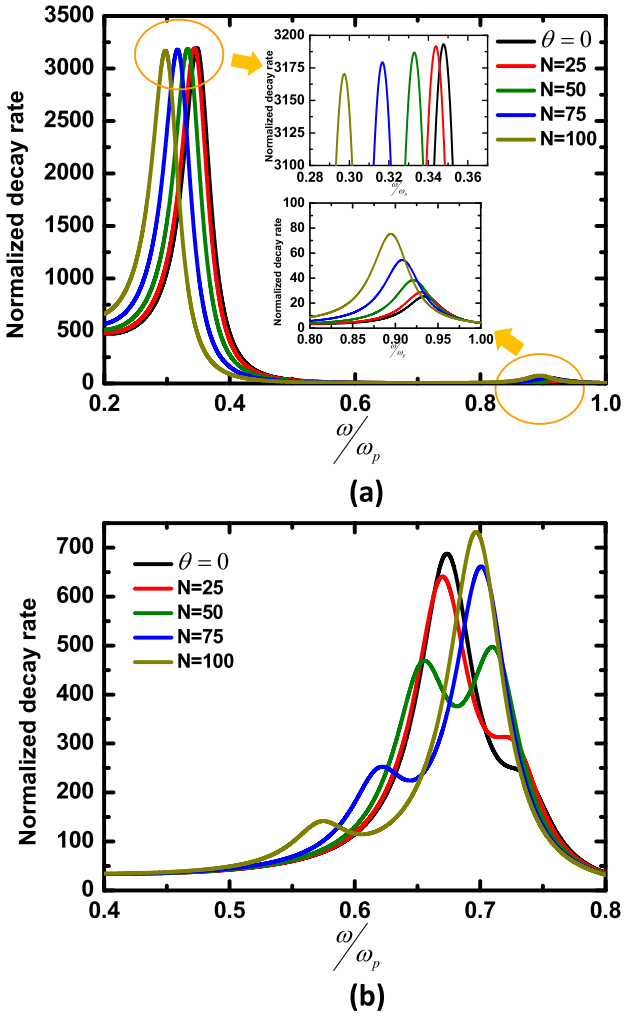

Fig. 3. Comparison between contributions to the decay rates from (a) the dipole ($\ell = 1$) mode and (b) a higher-multipole ($\ell = 11$) mode as a function of the normalized emission frequency $\frac{\omega}{\omega_p}$. Only the results for a radial dipole are shown.

tangental dipoles can experience large induced decay rates close to the nanoshell (with the radial dipole rates being even greater), they both drop rapidly as the emitter moves away. Most interestingly, one sees that the TME effects depend crucially on the emission frequency of the dipole. While for $\omega = 0.2\omega_p$ and for a fixed r_1, the decay rates will increase with the increase of N, those at $\omega = 0.6\omega_p$ will behave just in the opposite direction. This can again be accounted for from the different TME effect on the bonding and antibonding modes and for different multipole plasmons as can be seen from the peak and valley positions in the results shown from Fig. 2.

Discussion and conclusion

In this work, we have studied how an emitting dipole can be affected by a metallic nanoshell with a TI core with the application of axion electrodynamics in the long wavelength limit. In our numerical study, the value of N (hence the axion angle) is input as a parameter to manifest the TME, an approach following various previous studies in the literature on the TME induced optical scattering [19,20] and dipole emission phenomena [21]. At times, certain unrealistically large values of N have been used in our present and the previous studies to show more obvious manifestations of the TME. In practice, this can be adjusted by different methods including application of magnetic field normal to the TI; doping the TI with magnetic atoms; and coating the TI with a thin film of ferromagnetic materials. For the geometry of a spherical TI, the latter two methods seem to be more adaptable. More advanced fabrication methods for a time-reversal broken TI have been discussed recently in the literature [22]. In any case, such axion angle in a time-reversal broken TI will have values depending more significantly on these fabrication methods (e.g. the nature of the magnetic coating) besides on the alloyed TI materials [15,19]. As for the metal coating, the most significant geometric factor affecting the coupled plasmons across the metal shell is well-known to be the thickness of the shell. This effect has been well-studied in the literature of nanoshell plasmonics with ordinary dielectric core and we expect similar qualitative features for the case with a TI core, since the TME via the axion coupling to some extent can be accounted for via an effective dielectric response of a chiral medium. Hence it is expected that as the shell thickness decreases, the separation between the bonding and antibonding modes will increase with the former (latter) acquiring lower (higher) frequencies; while the plasmonic enhancement will become weakened [18].

From our analysis, some interesting modifications in the emission characteristics due to the TME response of a TI with broken time reversal symmetry have been revealed including significant red-shifts in the decay rate spectrum, and the possibility for both enhancing and suppressing of the decay depending crucially on the emission frequency of

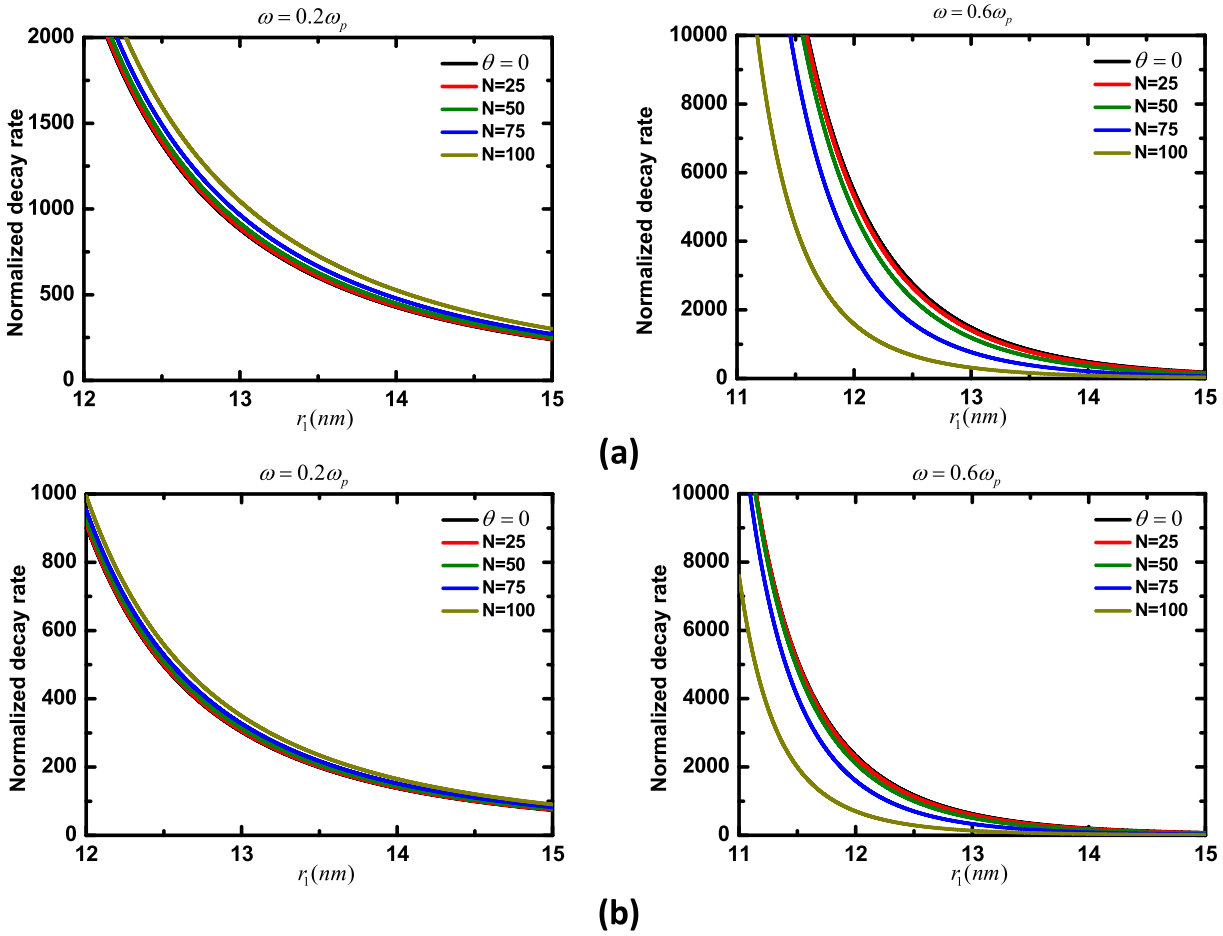

Fig. 4. Normalized decay rate of (a) radial and (b) tangential dipole near the nanoshell as a function of the distance r_1 from the center at fixed normalized emission frequency $\frac{\omega}{\omega_p} = 0.2$ and 0.6, respectively.

the dipole. In addition, the TME effect also is quite different on the bonding mode versus the antibonding modes of the coupled plasmons of the nanoshell. While it is our plan in a subsequent work to provide physical understanding of all these phenomena from application of a generalized plasmon hybridization model [23], with the incorporation of the axion field, our present results should be of interest in providing some guidance to experimenters to investigate the possibility of novel control of molecular fluorescing properties using these metal-coated TI particles.

Declaration of Competing Interest

The authors declare that they have no known competing financial interests or personal relationships that could have appeared to influence the work reported in this paper.

Acknowledgments

This work was supported by Technology, Institute of Nuclear Energy Research, Taiwan. We thank Mr. Mitikorn Wood-Thanan for his initial participation in this work.

References

[1] Hasan MZ, Kane CL. Rev Mod Phys 2010;82:3045.
[2] Qi XL, Zhang SC. Rev Mod Phys 2011;83:1057.
[3] Okada KN, et al. Nat Commun 2016;7:12245.
[4] Wu L, et al. Science 2016;354:1124.
[5] Dziom V, et al. Nat Commun 2017;8:15197.
[6] Xie HY, Leung PT. J Phys Commun 2020;4:095014.
[7] Karch A. Phy Rev B 2011;83:245432.
[8] Chang R, Xie HY, Wang YC, Chiang HP, Leung PT. Results Phys 2019;15:102744.
[9] Castro-Enriquez LA, Quezada LF, Martin-Ruiz A. Phys Rev A 2020;102:013720.
[10] Chatzidakis GD, Yannopapas V. Phys Rev B 2020;101:165410.
[11] Dulkeith E, Morteani AC, Niedereichholz T, Klar TA, Feldmann J, Levi SA, et al. Phys Rev Lett 2002;89:203002.
[12] Anger P, Bharadwaj P, Novotny L. Phys Rev Lett 2006;96:113002.
[13] Qi XL, Hughes TL, Zhang SC. Phys Rev B 2008;78:195424.
[14] Grushin AG, Cortijo A. Phys Rev Lett 2011;106:020403.
[15] Rodriguez-Lopez P. Phys Rev B 2011;84:165409.
[16] Because of this error, the values of N used in [8] in the plots of all the figures (N = 25, 50, 100) should correspond to (N ~ 80, 158, 315) after rounding off to the nearest integer. This change however has no effect on any of the discussion and conclusion of the original paper.
[17] Chance RR, Prock A, Silbey R. Adv Chem Phys 1978;1:37.
[18] Chang R, Leung PT. Phys Rev B 2006;73:125438.
[19] Zeng L, Song R, Zeng J, Dai C, Zhou Z. Optik 2013;124:4319.
[20] Ge L, Han D, Zi J. Opt Comm 2015;354:225.
[21] Song G, Xu J-P, Yang Y-P. EPL 2014;105:64001.
[22] Lee JS, Richardella A, Fraleigh RD et al. npj Quant Mater 2018; 3: 51.
[23] Prodan E, Nordlander P. J Chem Phys 2004;120:5444.